Applicable Analysis. Vol. 77(1–2), pp. 29–59
Reprints available directly from the Publisher
Photocopying permitted by license only

© 2001 OPA (Overseas Publishers Association) N.V.
Published by license under
the Gordon and Breach Science
Publishers imprint.
Printed in Malaysia.

Bifurcations in Ecosystem Models and their Biological Interpretation

Communicated by R.P. Gilbert

B.W. Kooi* and M.P. Boer†
Dept. of Theoretical Biology, Free University,
De Boelelaan 1087, 1081 HV Amsterdam, The Netherlands

Abstract

The use of bifurcation analysis for the study of the long-term dynamic behaviour of food webs is discussed. Food webs are collections of populations with often very complicated interactions. The non-viable nutrients are consumed by populations which are consumed by other populations at higher trophic levels, except for the top-predator species. In the most simple setting the dynamics of each population is described mathematically by an ordinary differential equation (ODE). In this paper we give an overview of local as well as global bifurcations found for a simple food web model. With chaotic behaviour all points in a next-return map appear to lie close to single curve. A cubic map with two critical points is studied and the results obtained are used to clarify global bifurcations of the ODE system. These global bifurcations are homoclinic bifurcations of a saddle limit cycle and a heteroclinic bifurcation from the equilibrium to the limit cycle. The homoclinic bifurcation of the saddle limit cycle is associated with a boundary crisis where a chaotic attractor is abruptly destroyed by a collision with the saddle limit cycle. The complex geometry of the basin of attraction of positive attractors is related to the existence of heteroclinic orbits. Furthermore, a homoclinic bifurcation for the saddle-focus equilibrium forms a 'skeleton' for the period doubling and tangent bifurcations of a limit cycle. Most results were already discussed in earlier papers; in this paper we emphasize the biological interpretations. For example, the transcritical bifurcations will be associated with invasion of species into an ecosystem.

AMS: 92D25, 37N25

KEY WORDS: Bifurcation analysis, chemostat, community assembly, food web, invasion, local and global bifurcation.

(Received for Publication February 2000)

*Corresponding author. Tel.:+31-20 44 47129; fax:+31-20 44 47123; e-mail: kooi@bio.vu.nl.
†Present address: Centre for Biometry Wageningen, Plant Research International, P.O. Box 16, 6700 AA Wageningen, The Netherlands, e-mail:M.P.Boer@plant.wag-ur.nl

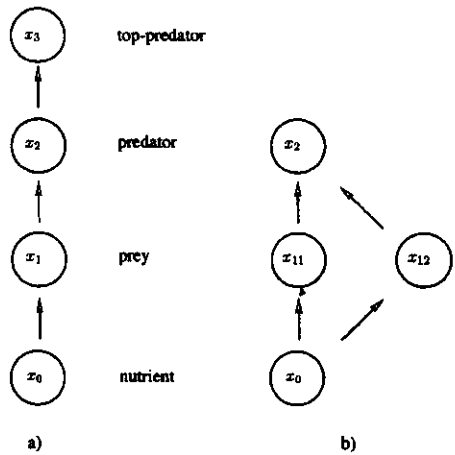

Figure 1: Food web structures with different trophic levels, x_i, $i = 1, 2, 3$ and a non-growing nutrient, x_0, at the base. The food chain a) with state variable x_i, $i = 1, 2, 3$ is studied in [3–5, 28, 29, 31]. The food web b) with state variables x_0, x_{11}, x_{12} and x_2 is discussed in [32].

1 Introduction

Food webs are ecosystems consisting of non-viable nutrients consumed by populations which are consumed by other populations at higher trophic levels, except for the highest level predator species (top-predator). With one population at each trophic level the ecosystem is called a food chain. In Figure 1.a we show the trophic graph of a tri-trophic food chain and in Figure 1.b of a simple food web.

We will give an overview of the study of the long-term dynamics of simple ecosystems. The model for these ecosystems is expressed in terms of a system of coupled ODEs and is analysed with dynamical system theory, especially bifurcation analysis; see for example [19, 33, 50]. The emphasis is on the bifurcation points in the parameter space where the dynamics changes abruptly when a parameter is varied. Detailed information on the asymptotic dynamical behaviour of the system is obtained in this way. In this paper we try to link mathematical concepts from bifurcation analysis to biological concepts and interpretations. The material of this paper consists of a combination of review and interpretation of past work and some new results.

The dynamics of bi-trophic and tri-trophic food chains, is studied intensively in the literature; we mention [5, 20, 21, 26, 27, 34, 41, 42]. Various types of complex dynamics, including chaotic behaviour, were found. In these models the lowest trophic level is viable (for instance it grows logistically) and this implies hidden assumptions about the availability of an abiotic nutrient.

In the bioenergetic food web models discussed in earlier articles [3, 4, 28, 29, 31], non-

reproducing nutrients at the base are modelled explicitly. These models obey mass conservation laws over the entire system (i.e. nutrients included) [30]. They can be formulated for various environmental conditions. We study a continuous flow culture with constant influx of the nutrient and a constant dilution rate for all trophic levels. The resulting mathematical model is an autonomous system of ODEs.

For a tri-trophic food chain in the chemostat, stable equilibria, periodic orbits and also complex, including chaotic, dynamic behaviour can occur. Also global bifurcations were found. First, a homoclinic bifurcation of a saddle-focus equilibrium where in the neighbourhood of this bifurcation in the parameter space the dynamics in time shows rather long periods close to a saddle-focus equilibrium. Homoclinic bifurcations of a saddle limit cycle are linked to boundary crises where a chaotic attractor disappears suddenly and converts into a chaotic transient, when a bifurcation parameter is varied, [18, 41]. Finally, heteroclinic orbits from the saddle-focus equilibrium with the saddle cycle are associated to the complex geometry of the boundary of the basin of attraction of limit cycles and strange attractors.

It is shown that the bifurcation structure of the food chain model for the region in the bifurcation parameter space where complex dynamics occurs, has much in common with the bifurcation structure of a one-dimensional map with two turning points. A cubic map is used to explain how attractors are created and destroyed under variation of bifurcation parameters.

In the ecological community assembly approach newly generated species or species from a finite pool of potential colonists, are added at random to an existing food web, starting with resources. The process by which ecosystems develop structure after colonizing a new area is also called *succession* [45]. A criterion determining whether a species can invade a food web is essential. In [35] Law and Morton propose a invasion criterion based upon a global criterion for coexistence of species, known as permanence, introduced by Hofbauer and Sigmund in [22]. In this paper this criterion is linked to transcritical bifurcations. This means that regions of invasibility in a bifurcation parameter space can be distinguished systematically and computer by the use of by available computer packages based on the bifurcation theory with the implementation of continuation techniques.

We will present calculated bifurcation diagrams for a tri-trophic nutrient–prey–predator–top-predator food chain, (see Figure 1.a) and a nutrient–two-competing prey–predator food web (see Figure 1.b). These systems are examples of simple ecological community systems. In both systems we deal with three populations, but in a different configuration.

Without predation two prey populations competing for the same nutrient, can coexist only when both species have exactly balanced parameters, a situation which cannot be expected to be found in nature. In [49] this phenomenon called *competitive exclusion* is discussed in this context. Under other conditions one competitor will win. Using bifurcation analysis we will study the implications of this phenomenon when a predator, consuming both competing prey populations, is introduced.

The applicability of the bifurcation analysis approach, focusing on invasion, in large-scale food webs as they can occur in natural ecosystems is discussed briefly.

2 Description of the models

This section presents a simple food web model. Let $x_0(t)$ denote the density of the nutrient (organic matter). Further, let $x_{ij}(t)$, $i = 1,2,3$, $j = 1,\cdots,N_i$ denote biomass densities of species j belonging to trophic level i where N_i is the number of species at that level. We introduce the total biomass at level i by $x_i = \sum_j^{N_i} x_{ij}$. When two trophic levels are involved in the definition of a parameter, two indices will be used separated by a comma. For instance, in general $\mu_{uv,ij}$ denotes the maximum growth rate of a predator x_{uv}, $u = 1,\cdots,n$ and $v = 1,\cdots,N_u$, feeding on a single prey population x_{ij}, $i = 1,2,3$ and $j = 1,\cdots,N_i$. With one species at a trophic level the second index is skipped.

A key component of models for the interaction of a predator and its prey is the relationship between the predation rate and the prey density, called the *functional response*. The (scaled) functional response of a predator, x_{ij} on prey x_{uv}, is assumed to be Holling type II, denoted by $f_{uv,ij} \in [0,1)$, with saturation constants $k_{uv,ij} > 0$ and is given by

$$f_{uv,ij} = \frac{x_{uv}/k_{uv,ij}}{1 + \sum_w x_{uw}/k_{uw,ij}} \,. \tag{1}$$

The prey is then consumed with a rate $I_{uv,ij} f_{uv,ij} x_{uv}$, where $I_{uv,ij} > 0$ is the maximum ingestion rate. This yields a growth rate of the predator equal to $\mu_{uv,ij} f_{uv,ij} x_{uv}$, where $\mu_{uv,ij} > 0$ is the maximum ingestion rate. Omnivory, when a predator consumes prey organisms from various trophic levels, is excluded and therefore we have $u = i - 1$.

With this (hyperbolic) functional response, the governing equations for the simple ecosystem with a nutrient, two prey, predator and top-predator, under chemostat conditions, is

$$\frac{dx_0}{dt} = (x_r - x_0)D - I_{0,11} f_{0,11} x_{11} - I_{0,12} f_{0,12} x_{12} \,, \tag{2a}$$

$$\frac{dx_{1j}}{dt} = x_{1j}\big(\mu_{0,1j} f_{0,1j} - D_{1j}\big) - I_{1j,2} f_{1j,2} x_2 \,, \quad j = 1,2 \,, \tag{2b}$$

$$\frac{dx_2}{dt} = x_2\big(\mu_{11,2} f_{11,2} + \mu_{12,2} f_{12,2} - D_2\big) - I_{2,3} f_{2,3} x_3 \,, \tag{2c}$$

$$\frac{dx_3}{dt} = x_3\big(\mu_{2,3} f_{2,3} - D_3\big) \,. \tag{2d}$$

We will not study the dynamics of the whole system, but that of two subsystems, a *food chain* and a *food web*. When $x_{12} = 0$, (see Figure 1.a) the food web structure reduces to a food chain with $x_1 = x_{11}$ in accordance with the notation introduced above. When $x_3 = 0$ the system is the simple food web (see Figure 1.b).

The depletion rate is the superposition of the dilution rate and the maintenance rate $D_{ij} = D + m_{ij}$. These terms D_{ij} can have different biological origins, for instance mortality rate, harvest rate or emigration rate. Here D is the dilution rate of the chemostat and $m_{ij} \geq 0$ is the so called maintenance rate. Then the term $m_{ij} x_{ij}$ is a depletion rate due to maintenance to keep the organism functioning. The resulting model (2) is called the Marr-Pirt or Monod-Herbert model. When $m_{ij} = 0$, $i = 1,2,3$, $j = 1,2$ this model is the Monod model, the classical model for microbial growth under chemostat conditions.

2.1 Boundedness

For nonlinear dynamical systems boundedness is very important. We will show boundedness by introducing a quantity which is inspired by biological interpretations, namely product formation. Observe that the imposed biological phenomena need not to hold true in nature; they are here used as guidelines in a mathematical proof.

Only a part of the amount of food ingested by species yields new biomass. For instance, population $i = 1$, $j = 1$ consumes substrate with a rate equal to $I_{0,11} f_{0,11} x_{11}$, a sink term in Equation (2a). The net growth rate of this population equates $\mu_{0,11} f_{0,11} x_{11}$, the source term in Equation (2b). Furthermore, part of the assimilated energy extracted from the substrate is used for maintenance, namely the sink term $x_{11} m_{11}$ in Equation (2b). The unusable parts form products which are ejected in the chemostat and they leave the reactor via the efflux with dilution rate D. This motivates the following expression for dissipated (unusable) mass densities p_1 produced by the two populations, $j = 1, 2$, at level $i = 1$ and expressed in the same units as the biomass densities x_i (with units for instance C-moles) by

$$\frac{dp_1}{dt} = \sum_{j=1}^{2} \Big(x_{1j} \big((I_{0,1j} - \mu_{0,1j}) f_{0,1j} + m_{1j} \big) \Big) - Dp_1 \,. \tag{3a}$$

For the predator population $i = 2$ consuming the two prey populations, $i = 1, j = 1, 2$ we have

$$\frac{dp_2}{dt} = x_2 \Big(\sum_{j=1}^{2} (I_{1j,2} - \mu_{1j,2}) f_{1j,2} + m_2 \Big) - Dp_2 \,, \tag{3b}$$

and similarly for the top-predator

$$\frac{dp_3}{dt} = x_3 \big((I_{2,3} - \mu_{2,3}) f_{2,3} + m_3 \big) - Dp_3 \,. \tag{3c}$$

The weighted total biomass density plus dissipated biomass density in the reactor may be defined by

$$H(t) = \sum_{i=0}^{3} x_i(t) + \sum_{i=1}^{3} p_i(t) \,, \; t \geq 0 \,. \tag{4}$$

For this quantity $H(t)$ we have

$$\frac{dH}{dt} = -D(H - x_r) \,, \quad H(t) = x_r + (H(0) - x_r) \exp\{-Dt\} \,. \tag{5}$$

Because the nutrient is supplied it is easy to show that the plane $x_0 = 0$ is repelling. The other boundary planes of the positive cone $(x_0 \geq 0, x_{11} \geq 0, x_{12} \geq 0, x_2 \geq 0, x_3 \geq 0) \in \mathbb{R}^5_+$ are invariant spaces. This is associated with non-spontaneous creation of life. Using theorems on uniqueness of the solution and inequalities for ODE systems, we can show that $x_i(t) \geq 0$, $i = 0, \cdots, 3$ and $p_i(t) \geq 0$, $i = 1, 2, 3$ when the inequalities holds for $t = 0$. Therefore we have

boundedness for $t \geq 0$, while the extended system converges asymptotically to the invariant manifold $H = x_r$.

With a food chain where the dynamics of all populations is described by the Monod model, that is $m_i = 0$, $i = 1, 2, 3$, it is advantageous to introduce the following function

$$K(t) = x_0(t) + \frac{I_{0,1}}{\mu_{0,1}} x_1(t) + \frac{I_{0,1} I_{1,2}}{\mu_{0,1}\mu_{1,2}} x_2(t) + \frac{I_{0,1} I_{1,2} I_{2,3}}{\mu_{0,1}\mu_{1,2}\mu_{2,3}} x_3(t) \ , \ t \geq 0 \ , \tag{6}$$

where the units of the biomasses x_i are now for instance gram and subsequently the maximum ingestion rate $I_{i-1,i}$ as gram ingested food per gram individual. For this quantity $K(t)$ we have the same expression as for $H(t)$ given in Equation (5)

$$\frac{dK}{dt} = -D(K - x_r) \ , \quad K(t) = x_r + (K(0) - x_r) \exp\{-Dt\} \ . \tag{7}$$

Thus, with the Monod food chain model, the dimension of the system can be reduced by one as far as the asymptotic behaviour is concerned. We can use $K = x_r$ to eliminate x_0 and, for a tri-trophic food chain, the remaining state variables are $x_i(t)$, $i = 1, 2, 3$. With the study of the basin of attraction we will use the Monod food chain model instead of the Marr-Pirt model.

3 Bifurcation analysis

Bifurcation analysis gives information about the long-term dynamic behaviour of nonlinear dynamic systems. The structural stability is studied with respect to so-called free or bifurcation parameters. In Table I the important bifurcation points are listed.

In Table II the basis bifurcation points for equilibria and limit cycles are summarized together with their normal forms for discrete-time systems (maps) and continuous-time systems of coupled ordinary differential equations (flows).

3.1 Discrete-time systems

Many of the earliest papers on chaos involved simple ecological systems of seasonally breeding populations with non-overlapping generations [38–40]. In these discrete time models the number of individuals in one year depends quadratically on the number of individuals in the previous year. This is the so called logistic map

$$y_{n+1} = r y_n (1 - y_n), \quad n \in \mathbf{N}, \quad r \in \mathbf{R}, \quad 0 \leq y_n \leq 1 \ , \tag{8}$$

where y_n is the population size in generation n and r is the intrinsic growth rate, which is the bifurcation parameter. This map is unimodal, that is there is one critical point where the derivative is zero.

Another classical discrete-time model in population biology is the Ricker model [46] given as

$$y_{n+1} = y_n \exp\{r(1 - y_n)\}, \quad n \in \mathbf{N}, \quad r \in \mathbf{R}, \quad y_n \geq 0 \ , \tag{9}$$

Table I: List of local and global bifurcations curves. Interior and boundary are both of the positive cone $\mathbf{R}_+^{i+1}$.

Bifurcation	Description
	Local bifurcations
$T_{e,i}$	Tangent bifurcation: collision of two equilibria
$T_{c,i}$	Tangent bifurcation: collision of two limit cycles
$TC_{e,i}^{\pm}$	transcritical bifurcation: invasion through boundary equilibrium, origin of stable (supercritical, $\pm = -$) or unstable (subcritical, $\pm = +$) interior equilibrium
$TC_{c,i}^{\pm}$	Transcritical bifurcation: invasion through boundary limit cycle, origin of stable (supercritical, $\pm = -$) or unstable (subcritical, $\pm = +$) interior limit cycle
$H_i^{\pm}$	Hopf bifurcation: equilibrium becomes unstable, origin of stable (supercritical, $\pm = -$) or unstable (subcritical, $\pm = +$) limit cycle
$F_i^{\pm}$	flip bifurcation: period doubling of limit cycle origin of stable (supercritical, $\pm = -$) or unstable (subcritical, $\pm = +$) period-2 limit cycle
$Z_{e,2}$	Bifurcation with zero eigenvalues: extinction of the predator
	Global bifurcations
$G_e^{=}$	Homoclinic bifurcation for equilibrium Shil'nikov bifurcation, skeleton for flip and tangent bifurcations
$G_c^{=}$	Homoclinic bifurcation for limit cycle boundary crisis, skeleton for flip and tangent bifurcations
$G_{e,c}^{\neq}$	Heteroclinic bifurcation for equilibrium to limit cycle complex geometry of the basin boundary in state-space

Table II: List of the basic codimension-one local bifurcations for ODEs: $dx/dt = f(x, \alpha)$, and maps: $y_{n+1} = f(y_n, \alpha)$ with their normal form. $\alpha \in \mathbb{R}$ is the bifurcation parameter and $\alpha = 0$ the bifurcation point. λ is the eigenvalue of the Jacobian matrix evaluated at the equilibrium $x = 0$. μ is the Floquet multiplier, that is the eigenvalue of the monodromy matrix of the Poincaré next-return map, and evaluated at the limit cycle such that $y_n = 0$ is a fixed point.
With food web dynamics, a stable positive attractor originates at a supercritical, $^-$, transcritical bifurcation and an unstable positive equilibrium or limit cycle at a subcritical, $^+$, transcritical bifurcation.

Bif.	Description	normal form	characteristic exponents
T_e	Tangent bifurcation;	$dx/dt = \alpha - x^2$	Re $\lambda = 0$
T_c	Tangent bifurcation;	$y_{n+1} = y_n + \alpha - y_n^2$	Re $\mu = 1$
$TC_e^{\pm}$	Transcritical bifurcation;	$dx/dt = \alpha x \pm x^2$	Re $\lambda = 0$
$TC_c^{\pm}$	Transcritical bifurcation;	$y_{n+1} = (1+\alpha)y_n \pm y_n^2$	Re $\mu = 1$
$H^{\pm}$	Hopf bifurcation;	$dx/dt = -y + x(\alpha \pm (x^2+y^2))$	
		$dy/dt = x + y(\alpha \pm (x^2+y^2))$	Re $\lambda_{1,2} = 0$
$F^{\pm}$	Flip bifurcation;	$y_{n+1} = -(1+\alpha)y_n \pm y_n^3$	Re $\mu = -1$

where, just as in the logistic map (8), y_n is the population size in generation n and r is also called the intrinsic growth rate. This model was used in a recent paper [24] as a starting point for the modelling of host-parasitoid interaction where the dynamics of the host population and the parasite population were described by the Ricker model. They found for this two-dimensional system, that several types of attractors may coexist, including quasi-periodic and chaotic attractors. Furthermore, the boundaries of the basin of attraction may have complex geometrical properties. The basin of attraction of an attractor is defined as the set of initial conditions whose trajectories asymptotically approach the attractor as time increases [18].

A modified Ricker model was used in [14] to study the evolutionary competition of phenotypes of a semelparous species, which means that individuals reproduce only once and then die. Heteroclinic tangencies were found for this system. This global bifurcation was associated with the boundary of a region were a striking biological phenomenon exists, namely "the resident–strikes–back". Initially a mutant can invade the resident population but finally it goes extinct and the resident remains.

The following one-dimensional discrete-time system will be considered to explain global bifurcations for a saddle limit cycle of the ODE system (2):

$$y_{n+1} = f_{\alpha,\beta}(y_n) = 16\beta y_n^3 - 24\beta y_n^2 + 9\beta y_n + \alpha - \beta, \quad n \in \mathbf{N}, \quad \alpha,\ \beta \in \mathbf{R}\,, \tag{10}$$

where $y_n \in \mathbf{R}$ is the state at time n and $f_{\alpha,\beta} : \mathbf{R} \to \mathbf{R}$ a non-invertible function. This map and a two-dimensional invertible extension $y_{n+1} = f_{\alpha,\beta}(y_n) - \varepsilon y_{n-1}$, with ε a small positive scalar, are studied in detail in [3]. The map $f_{\alpha,\beta}$ has two turning points (and is therefore called a bi-modal map), $c_1 = \frac{1}{4}$ and $c_2 = \frac{3}{4}$, where $f(c_1) = \alpha$ is a local maximum and $f(c_2) = \alpha - \beta$ is a local minimum. The dynamics of this cubic map can be analysed in great detail, using an extensive

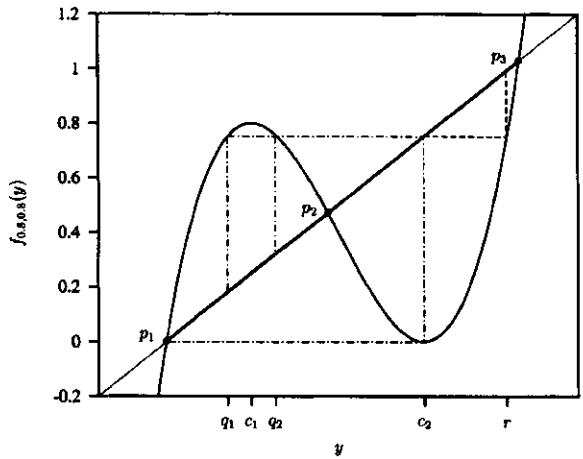

Figure 2: The function $f_{\alpha,\beta}$ for $\alpha = 0.8$ and $\beta = 0.8$. The points p_1, p_2, and p_3 are fixed points of system (10). The map has turning points at c_1 and c_2. The orbits starting at points q_1 and q_2 are degenerate homoclinic orbits: $f^2_{0.8,0.8}(q) = p_1$ and $\lim_{n\to-\infty} f^n_{0.8,0.8}(q) \to p_1$ for $q \in (p_1, c_1)$. The orbit starting at point r is a degenerate heteroclinic orbit: $f^2_{0.8,0.8}(r) = p_1$ and $\lim_{n\to-\infty} f^n_{0.8,0.8}(r) \to p_3$ for $r \in (c_2, p_3)$. The solid interval on the diagonal is the basin of attraction.

theory [11,13,37,48,51]. In Figure 2 the map $f_{\alpha,\beta}$ is given for $\alpha = \beta = 0.8$. For these parameter values, map (10) has three fixed points, denoted by p_1, p_2, and p_3, with $p_1 < p_2 < p_3$ and is invariant on the interval $[p_1, p_3]$. Restricted to one of the intervals (p_1, c_1), (c_1, c_2) and (c_2, p_3) the map $f_{\alpha,\beta}$ is invertible. The fixed points p_1 and p_3 are repellors. Then with $q \in (p_1, c_1)$ we have $\lim_{n\to-\infty} f^n_{0.8,0.8}(q) \to p_1$ and with $r \in (c_2, p_3)$ we have $\lim_{n\to-\infty} f^n_{0.8,0.8}(r) \to p_3$. The local stability of point p_2 is not considered here, since this is unimportant for our present purposes. An orbit starting at a point $q \in (p_1, c_1)$ ($q \in (c_2, p_3)$) is called *homoclinic* to p_1 (p_3) if there exists $n > 0$ such that $f^n(q) = p_1$ ($f^n(q) = p_3$). Starting at a point $r \in (c_2, p_3)$ ($r \in (p_1, c_1)$) the orbit is called *heteroclinic* from p_3 to p_1 (p_1 to p_3) if there exists $n > 0$ such that $f^n(q) = p_1$ ($f^n(q) = p_3$); see for instance [13].

A one-parameter bifurcation diagram with α as the bifurcation parameter is shown in Figure 3 for $\beta = 0.8$. It is point-symmetric with respect to the point $(\alpha, y) = ((1+\beta)/2, 1/2) = (0.9, 0.5)$. The unstable equilibrium values p_1 and p_3 are plotted.

At the tangent bifurcation point T, at $\alpha \approx 0.2255$, the heteroclinic orbits together with the basin of attraction and the fixed points p_1 and p_2 disappear. In the region between this tangent bifurcation T and homoclinic bifurcation point ($\alpha \approx 0.5361$) denoted by $G^=$ the bifurcation diagram resembles the well-known bifurcation diagram of the logistic map (8) for $r \in [1, 4]$

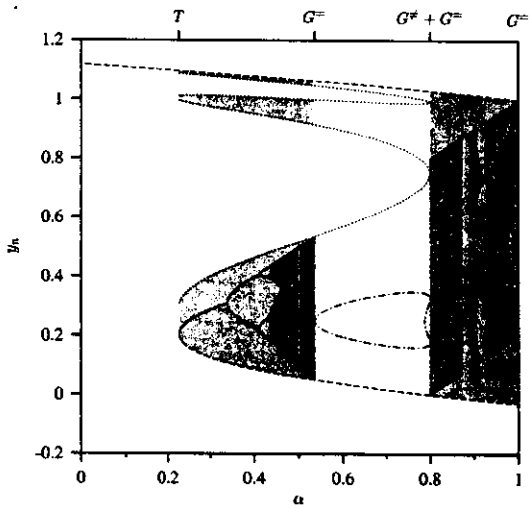

Figure 3: One-parameter bifurcation diagram of the one-dimensional system (10) for $\beta = 0.8$. The dashed curves indicate the repellors p_1 and p_3. The points on the dotted curves lie on a heteroclinic orbit. The points on the dashed-dotted curve lie on a homoclinic orbit. The attractors are plotted as points. The grey regions are the basin of attraction of these attractors. This diagram is point-symmetric with respect to point $(0.9, 0.5)$.

discussed in [39]. Restricted to the invariant interval $y \in [p_1, r_1]$ it is essentially an unimodal map with one critical point similar to the logistic map.

For increasing α the fixed point becomes unstable and a cascade of period doubling leads to chaotic dynamics. As with the unimodal logistic map for $r = 4$, the strange attractor disappears suddenly at a homoclinic bifurcation point. In Figure 4 the map for $\alpha = 0.5361$ is shown. The homoclinic orbits to the equilibria p_1 for $\alpha \gtrapprox 0.5361$ are similar to those occurring for the logistic map (8) for $r > 4$. At the global bifurcation point these homoclinic orbits for $\alpha \geq r_1$ become degenerate ($f'(y) = 0$ for at least one point y on the orbit) and this orbit is shown in Figure 4.

In the "hole" $0.5361 \lessapprox \alpha < 0.8$ homoclinic orbits exist. Notice that if y is on a homoclinic orbit than also $f^n(y)$ for each $n \geq 1$ but that only those points y with $f^2(y) = p_1$ are plotted in the one-parameter bifurcation diagram Figure 3.

In the interval $\alpha \in [0.8, 1.0]$ there is chaotic dynamics with an abrupt destruction of the chaotic attractor and its basin of attraction at the end points of this interval in $\alpha = 0.8$ and $\alpha = 1.0$. Here homoclinic orbits to the equilibria p_1 and p_3, respectively, become degenerate at the global bifurcation point (see Figure 2). With $\alpha = (1 + \beta)/2$ the equilibria p_3 and p_1 switch role.

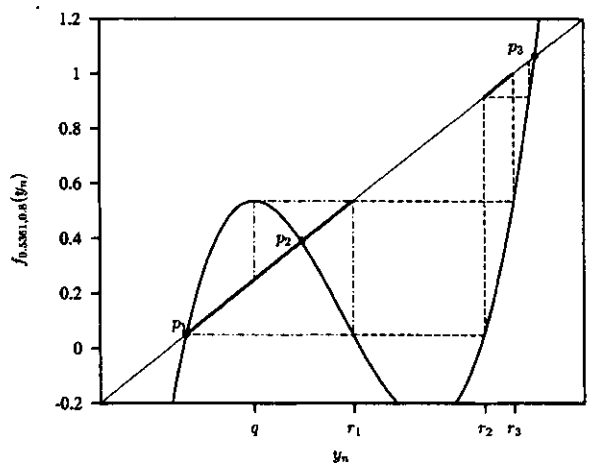

Figure 4: The function $f_{\alpha,\beta}$ for $\alpha = 0.5361$ and $\beta = 0.8$. The points p_1, p_2, and p_3 are fixed points of system (10). The map has one turning point in the invariant interval (p_1, r_1). The orbit starting at point q is a degenerate homoclinic orbit: $f^2_{0.5361,0.8}(q) = p_1$ and $\lim_{n\to-\infty} f^n_{0.5361,0.8}(q) \to p_1$ for for $q \in (p_1, c_1)$). The orbit starting at point r_2 and r_3 are heteroclinic orbits: $f_{0.5361,0.8}(r_2) = p_1$ and $f^2_{0.5361,0.8}(r_3) = p_1$ while $\lim_{n\to-\infty} f^n_{0.5361,0.8}(r) \to p_3$ for $r \in (c_2, c_3)$. The solid intervals on the diagonal are in the basin of attraction, the endpoints are on heteroclinic orbits.

In the one-parameter bifurcation diagram Figure 3 also points on a heteroclinic orbit which connects the points p_3 and p_1 are plotted in the interval $\alpha \in [\approx 0.2255, 0.8]$. At the global bifurcation point denoted by $G^{\neq}$ the heteroclinic orbits between points p_3 and p_1 become degenerate. For $\alpha = 0.5361$ the heteroclinic orbits are also depicted in Figure 4.

In the Figures 2, 3 and 4 the basin of attraction is also shown. With no heteroclinic orbits, $\alpha \in [0.8, 1.0]$, the basin is connected. However, with heteroclinic orbits $\alpha \in [\approx 0.2255, 0.8]$ convergence to a positive attractor for $\alpha \in [\approx 0.2255, 0.5361]$ occurs in disconnected intervals with endpoints on heteroclinic orbits (see Figure 4) and close to the equilibrium p_3 the basin boundary has a complex geometry. At the tangent bifurcation point T the boundary basin is a vertical line where α is constant, that is the basin of attraction disappears abruptly at the tangent bifurcation together with the fixed points p_1 and p_2.

The results obtained for the map (10) will be used to clarify global bifurcations for a saddle limit cycle in the tri-trophic food chain model studied in Section 5.

Table III: Parameter set for bacterium-ciliate models, after [9]. The values for the new parameters m_i are also given. The ranges for the control parameters are $0 < D < \mu_{0,11}$ and $0 < x_r \leq 300$ mg dm^{-3}. The reference values for the perturbation parameters are: $\epsilon_1 = -0.08$ h^{-1}, $\epsilon_2 = 0.1$ h^{-1} and $\delta_1 = -2.5$ mg dm^{-3}, $\delta_2 = 0.1$ mg dm^{-3}. Time budget models where search and handling times are distinguished can be used to derive the Holling type II functional response for multiple resources (see [43]). For the sake of simplicity we take $\gamma_1 = 0$ h^{-1} and $\gamma_2 = 0$ h^{-1}.

parameter	unit	values				
		$i=1$		$i=2$		$i=3$
		$l=1$	$l=2$	$j=1$	$j=2$	
$\mu_{(i-1)j,il}$	h^{-1}	0.5	$0.5+\epsilon_1$	0.2	$0.2+\epsilon_2$	0.15
$k_{(i-1)j,il}$	mg dm^{-3}	8	$8+\delta_1$	9	$9+\delta_2$	10
$I_{(i-1)j,il}$	h^{-1}	1.25	$1.25+\gamma_1$	0.33	$0.33+\gamma_2$	0.25
m_{il}	h^{-1}	0.025		0.01		0.0075

3.2 Continuous-time systems

The Lorenz model [36] is the well-studied autonomous system of three first order ODEs which shows chaotic behaviour as well as boundary crises, [17].

With food chains, it can be proved using a Lyapunov function, that for a general Lotka-Volterra food chain model (Figure 1.a) in the absence of competition within predators, there is global stability to an interior equilibrium, if it exists [22, page 64].

Gilpin [16] was the first to find chaos in a food web consisting of two coexisting prey and one predator. This food web has a trophic graph given in Figure 1.b where the nutrient is not modelled explicitly. The dynamics of each population is still described by general Lotka-Volterra equations with no competition within the predator population. The dynamics of bi-trophic and tri-trophic food chains with a Holling type II instead of the Lotka-Volterra functional response is studied in detail in [20, 21, 26, 27, 34, 42]. Various types of complex dynamics, including chaotic behaviour, were found. In [10] a singular perturbation analysis was used to prove that the tri-trophic food chain model possesses a homoclinic bifurcation. Homoclinic orbits of the Shil'nikov type and a boundary crisis were found in [41,42]. This shows that complex dynamics can be the result of a more complex trophic graph but also caused by more complex interactions between the populations.

In sections 4 and 5 we will give an overview of previous work on the dynamics of a food chain under chemostat conditions, where nutrients are modelled explicitly. For a fixed composition of the species in the food chain, the bifurcation parameters are the environmental parameters. In the chemostat case these are the dilution rate, $D > 0$, and the concentration of nutrients in the influx, $x_r \geq 0$, which are under control of the experimenter. The parameter settings given in Table III are realistic for a microbial food chain.

The bifurcation software packages LOCBIF [25] and AUTO [15] were used to calculate the local bifurcation curves in the bifurcation diagrams. These were calculated as follows. First one

calculates with fixed parameter values a positive attractor, often a stable equilibrium. Using a continuation technique with one parameter free a point on a codimension-one bifurcation curve is found. Starting at this point this curve is continued while test functions which are indicative of codimension-two bifurcation points are checked. For higher codimension bifurcations curves the same procedure can be followed.

Besides local bifurcations also global bifurcation occur. Let the flow $\phi(t,x)$, $\phi : \mathbf{R} \times \mathbf{R}^n_+ \to \mathbf{R}^n_+$, denote a solution of governing system of n ODEs such that $\phi(0,x) = x$. With a homoclinic orbit there is convergence to an unstable equilibrium or limit cycle for $t \to \infty$ as well as $t \to -\infty$, that is $\phi(t,x) \to X$ for $t \to \pm\infty$ where X denotes an equilibrium or limit cycle. With heteroolinic orbits the convergence for $t \to \infty$ and $t \to -\infty$ is to different equilibria or limit cycles. We computed the heteroclinic and homoclinic orbits with a boundary-value method [1, 2, 6, 8]. Such a method truncates a heteroclinic or homoclinic orbit to a finite time interval and impose certain boundary conditions at the end points of that interval. Suitable boundary conditions are obtained by using linear approximations of the stable and unstable manifolds near the equilibrium or limit cycle.

Bifurcation points for homoclinic orbits are denoted by $G^{=}_{e}$ when homoclinic orbits to an equilibrium point are involved and by $G^{=}_{c}$ when it is to a limit cycle. Bifurcations of heteroclinic orbits are denoted by $G^{\neq}_{e,c}$ when they are from a equilibrium point to a limit cycle as time increases and by $G^{\neq}_{c,e}$ from a limit cycle to an equilibrium. All global bifurcations were calculated and continuated in the two-parameter x_r, D-space with the numerical techniques described in [5].

The program HOMCONT being part of the AUTO package [15] was also used for continuation of the homoclinic global bifurcation, $G^{=}_{e}$, to the saddle-focus equilibrium. The theory is described in [6, 7] and [33, page 467].

4 Bi-trophic food chain

We study the dynamics of system (2) with $x_{12} = 0$ and $x_3 = 0$, thus in the positive cone $(x_0 \geq 0, x_1 \geq 0, x_2 \geq 0) \in \mathbf{R}^3_+$.

In Figure 5 we show the bifurcation diagram for a bi-trophic food chain (nutrient–prey–predator system) where the dynamics of each population is described by the Marr-Pirt model. There are three important regions, a region where the predator goes to extinction (left-hand side of $TC^{-}_{e,2}$), a region with a stable equilibrium (at the right-hand side of $TC^{-}_{e,2}$ and at the left-hand side of H^{-}_{2}) and a region where a stable limit cycle exists (to the right of H^{-}_{2}). We stress that for other values of the parameters given in Table III or different ranges of the bifurcation parameters used in Figure 5, more complex asymptotic dynamic behaviour can occur.

4.1 Invasibility

The curves $TC^{-}_{e,1}$ and $TC^{-}_{e,2}$ are (supercritical) transcritical bifurcation curves. It can be shown that a species can invade a system if its per capita growth rate is larger than its depletion rate with its population biomass density zero while the other species are at their equilibrium values. Thus

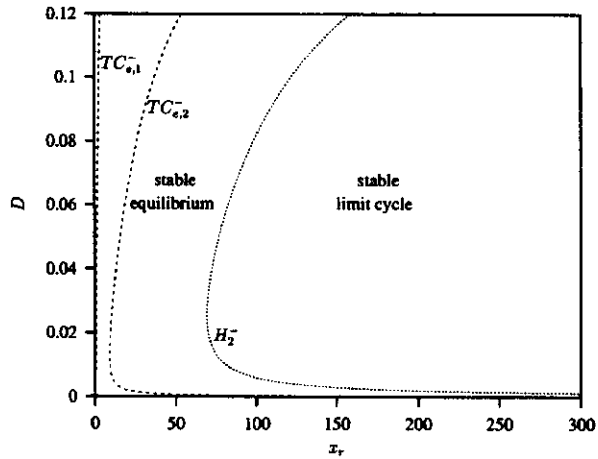

Figure 5: Bifurcation diagram for Marr-Pirt model of bi-trophic food chain, system (2) without competition. The bifurcation parameters are the dilution rate D and the substrate concentration in reservoir x_r. Values assigned to physiological parameters and reference values for the perturbation parameters are listed in Table III. The curves $TC^-_{e,1}$, $TC^-_{e,2}$ are supercritical transcritical bifurcation curves and H^-_2 marks a supercritical Hopf bifurcation curve.

invasion is possible when the initial rate of increase of the invading species is positive. For a Lotka-Volterra food web this holds true irrespective of whether the attractor of the virgin system is a fixed point or a periodic or chaotic orbit [44]. Another criterion, which holds when the rate of the change of the population biomass density is proportional to the biomass density itself (sometimes called the Kolmogorov property), uses an eigenvalue analysis. The Lyapunov exponent associated with the dynamics of the invader has to be positive on the boundary attractor. Thus, the transcritical bifurcation point, where the Lyapunov exponent is zero, marks the region where invasion is possible. The latter criterion is used in this paper to calculate the boundaries of the regions in the bifurcation diagram where the species compositions of the food web changes. With the super(sub)critical transcritical bifurcations the originating positive attractor is (un)stable.

In physics transcritical bifurcations require often an extra constraint, [50], but in biological applications not, since biomasses have to be positive which ensures realism. Spontaneous creation is not allowed and therefore the boundary planes $x_i = 0, i > 0$ are invariant.

4.2 Paradox of enrichment

Curve H_2^- marks a supercritical Hopf bifurcation curve. The transition over the supercritical Hopf bifurcation curve, H_2^-, due to an increase in the nutrient supply is associated with the paradox of enrichment [47]. It marks the rate at which nutrients are supplied at the bottom of the food chain where the ecosystem becomes unstable, which leads to cyclic behaviour. Instability of the equilibrium is obtained if the prey population, x_1, can overcome the control imposed by both the competition for nutrients, x_0, and the predatory pressure, x_2 (see [4]). De Roos *et al.* [12] called this destabilizing mechanism the *prey escape mechanism*.

5 Tri-trophic food chain

We explore the dynamics of system (2) with $x_{12} = 0$ in the positive cone $(x_0 \geq 0, x_1 \geq 0, x_2 \geq 0, x_3 \geq 0) \in \mathbb{R}^4_+$. Figure 6 gives the bifurcation diagram. Observe that also the bifurcation curves of the bi-trophic food chain (Figure 5) are part of the diagram because of the hierarchical structure of a food chain. When a top-predator is introduced the equilibria and periodic orbits of the virgin system remain equilibria and periodic orbits also for the extended system, but can become unstable. Furthermore, multiple attractors are possible, in the interior of the positive cone for the tri-trophic food chain, and at the exterior, thus at the boundary of the positive cone, for the bi-trophic food chain.

There is an "organizing center", namely the codimension 2 point M_1. In this point one real and the real part of two complex conjugated eigenvalues of the Jacobian evaluated in the equilibrium are zero. In Figure 6 the transcritical curves $TC^{\pm}_{e,3}$ and $TC^{\pm}_{c,3}$ for equilibria and limit cycles where $x_3 = 0$, originating from M_1 are given. Observe that with $TC^-_{e,3}$ between the points M_1 and M_2 there are two complex conjugated eigenvalues with a positive real part besides the zero eigenvalue. Thus, in this case the originating positive attractor is unstable for a supercritical transcritical bifurcation, $TC^-_{e,3}$. In the points M_2 and M_3 the supercritical transcritical bifurcations $TC^-_{e,3}$ and $TC^-_{c,3}$ become subcritical, $TC^+_{e,3}$ and $TC^+_{c,3}$, respectively. Because in this region of the diagram the bi-trophic food chain has a stable limit cycle, only the transcritical bifurcation $TC^-_{c,3}$ is important for invasibility and not the transcritical bifurcation $TC^-_{e,3}$ of the unstable equilibrium of the bi-trophic food chain. In the points M_2 and M_3 tangent bifurcation curves originate for equilibria, $T_{e,3}$, and limit cycles, $T_{c,3}$. At the tangent bifurcations a pair of interior equilibria or limit cycles disappears simultaneously. In the points M_2 and M_3 this occurs for $x_3 = 0$. The tangent bifurcation curve $T_{c,3}$ has a cusp bifurcation point. The bifurcation curve has two branches with a common tangent in the cusp point. This type of bifurcation is often associated with *catastrophes*.

Figure 7 is an expanded picture of Figure 6 in the region were complex dynamics occurs. There are three global bifurcations, namely homoclinic bifurcations of a saddle-focus equilibrium $G^=_e$ and saddle limit cycle $G^=_c$ as well as a heteroclinic bifurcation $G^{\neq}_{e,c}$ from the equilibrium to the limit cycle. There are codimension-two points for the intersection of the homoclinic bifurcation curve $G^=_e$ with the homoclinic bifurcation curve $G^=_c$ and with the heteroclinic bifurcation curve $G^{\neq}_{e,c}$.

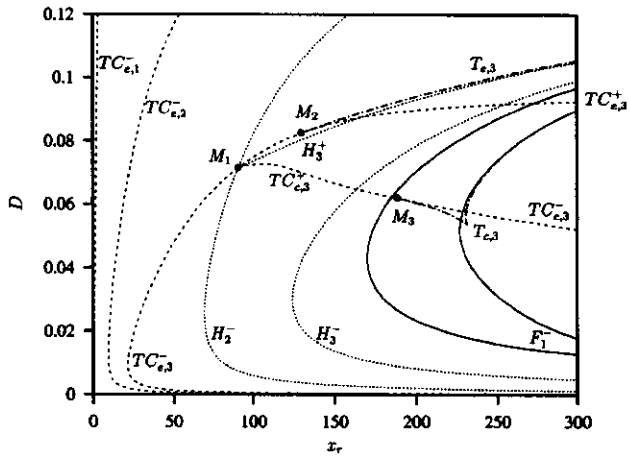

Figure 6: Bifurcation diagram for Marr-Pirt model of tri-trophic food chain, system (2) without competition. The bifurcation parameters are the dilution rate D and the substrate concentration in reservoir x_r. Values assigned to physiological parameters and reference values for the perturbation parameters are listed in Table III.

Now we focus our attention on the one-parameter bifurcation diagram for the local maxima of the top predator x_3 shown in Figure 8. The free parameter is the dilution rate while the concentration substrate in the reservoir is fixed at $x_r = 250$. In order to get rid of the transients, integration is performed for a fixed time without examination of the results. From that point in time the biomass of the top predator peak value is shown as a dot in the diagram. At the top the rotated bifurcation diagram Figure 6 is plotted for $225 \leq x_r \leq 250$. Bifurcation points (the dilution rates for intersection points in two-parameter diagram, Figure 6, of bifurcation curves with $x_r = 250$ line) are indicated by vertical lines in the one-parameter bifurcation diagram Figure 8.

For D values slightly larger than 0.1 there is a tangent bifurcation $T_{e,3}$ where two internal equilibria collide. Both equilibria are unstable. The biomass of the top-predator at the lowest unstable equilibrium becomes zero at the subcritical transcritical bifurcation $TC^+_{e,3}$. The unstable equilibrium can act as a separatrix; below this line the top-predator goes extinct and above this line it converges to the internal attractor if it exists. This shows that with the subcritical transcritical bifurcation when the top-predator can invaded, the orbit converges to a positive attractor possibly far from the boundary of the state space ("catastrophic" change). Notice that the equilibrium on the boundary represents an unstable bi-trophic food chain (see Figure 5) and therefore it cannot represent an intermediate stage in a succession.

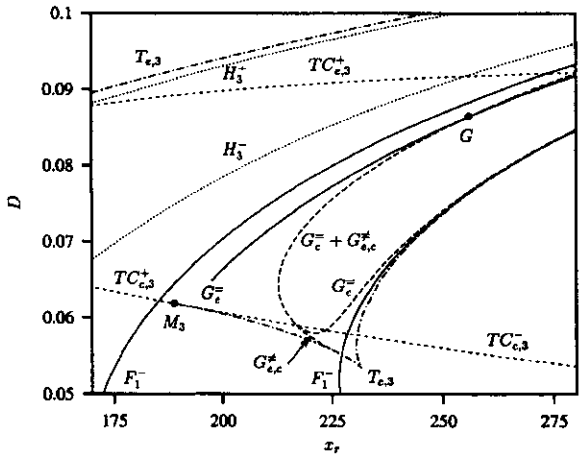

Figure 7: Detail of the bifurcation diagram for Marr-Pirt model of tri-trophic food chain given in Figure 6. Homoclinic $G_e^=$, $G_c^=$ and heteroclinic $G_{e,c}^{\neq}$ bifurcation curves denote global bifurcations. Point G is the intersection of the homoclinic bifurcation curves $G_e^=$ with the heteroclinic bifurcation curve $G_{e,c}^{\neq}$.

The equilibrium with the largest value for x_3 becomes stable for D values slightly lower than 0.1 at a subcritical Hopf bifurcation H_3^+. With decreasing D there is coexistence of a positive equilibrium, denoted by E_p, and an unstable limit cycle, denoted by L_p. This equilibrium becomes unstable again and a stable limit cycle originates at the supercritical Hopf bifurcation H_3^-. With decreasing D, a cascade of period doubling leads to chaotic behaviour.

There is a stable interior limit cycle for D values below the supercritical transcritical bifurcation for limit cycles $TC_{c,3}^-$ value. Above we mentioned that the equilibrium on the boundary above the subcritical transcritical bifurcation $TC_{e,3}^+$ was unstable if regarded as a bi-trophic food chain. There is a stable limit cycle, but because the D-value is also above the supercritical transcritical bifurcation $TC_{c,3}^-$ invasion of the top-predator via that limit cycle is still impossible.

With decreasing values of D this limit cycle becomes unstable at a (supercritical) flip bifurcation F_1^-, and then stable again at the flip bifurcation F_1^- before it disappears with the supercritical Hopf bifurcation H_3^-. Flip and tangent bifurcation curves for period-2 and higher periods are not shown.

For rather small D-values in Figure 8 the equilibrium top-predator biomass becomes zero at the supercritical transcritical bifurcation $TC_{e,3}^-$. Varying the bifurcation parameter the supercritical transcritical bifurcation marks a point where the top-predator can invade and there is convergence to a positive attractor close to the boundary of the state space ("non-catastrophic" change).

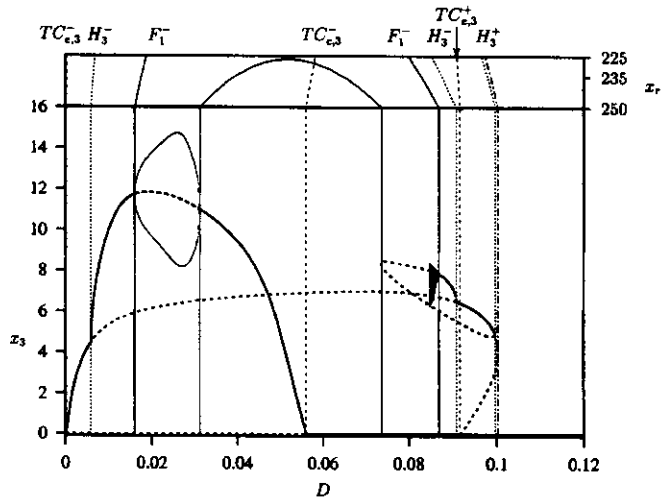

Figure 8: One-parameter bifurcation diagram for Marr-Pirt model of tri-trophic food chain, system (2) without competition. The maximum values for the top-predator density x_3 are plotted as a function of the dilution rate D. The concentration in the reservoir is $x_r = 250$. Solid curves give stable equilibrium values and peak values of stable limit cycles. Dashed curves give unstable equilibrium values. At the top a part of the the rotated two-parameter bifurcation diagram, Figure 6, is plotted for $225 \leq x_r \leq 250$.

Figure 9 gives also a one-parameter bifurcation diagram for the Marr-Pirt model of a tri-trophic food chain, but now the concentration in the reservoir is $x_r = 235$ instead of 250. The local minima are plotted instead of maxima and also global bifurcations are indicated.

There is a "hole" in the chaotic attractor between the global bifurcations $G^=_c$. For two values of the dilution rate D close to the homoclinic global bifurcation point, $G^=_c$ with $D \approx 0.08$, a next-minimum map of x_3 was constructed in Figure 10. For the D-value above the homoclinic bifurcation point there is a positive chaotic attractor. For the D-value below the homoclinic bifurcation point we have a chaotic transient. That is, the biomasses vary in a chaotic fashion and then without warning the top-predator biomass density x_3 drops rapidly to zero.

The local minima in the graphs of Figure 10 lie close to a single curve. This indicates that the chaotic attractor is almost one-dimensional. It has two turning points, *i.e.* the map has a local maximum and a local minimum. Two maps with a negative Schwarzian derivative [13, 19, 48] and the same number of turning points, have basically the same bifurcation structure [13, 37, 51]. This allows for the study of the chaotic attractor of system (2) without competition ($x_{12} = 0$) as shown in Figure 10 by a simple cubic map. We have chosen the map (10) discussed above, to present the relationship between the bifurcation structures of continuous-time system (flow) and the discrete-time (map) system, connected by the Poincaré mapping.

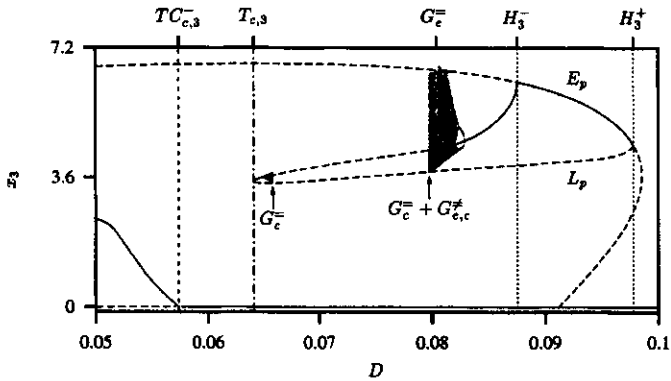

Figure 9: One-parameter bifurcation diagram for Marr-Pirt model of tri-trophic food chain, system (2) without competition. The minimum values for the top-predator density x_3 are plotted as a function of the dilution rate D. The concentration in the reservoir is $x_r = 235$. Plotted as points are the local minima or constant values of x_3 of the attractors versus dilution rate D. The dashed lines indicate unstable limit cycles or unstable equilibria. There are two global bifurcations, indicated with $G^=_c$ and $G^{\neq}_{c,c}$.

We will present results for the Monod model tri-trophic food chain when the basin of attraction, being a region in state space, is studied. With the Monod model, we have $m_i = 0$, $i = 1, 2, 3$. Then Equation (7) gives $K(t) = x_r$ when $K(0) = x_r$. Thus we can eliminate the nutrient density with Equation (6): $x_0 = x_r - (\frac{I_{0,1}}{\mu_{0,1}}x_1 + \frac{I_{0,1}I_{1,2}}{\mu_{0,1}\mu_{1,2}}x_2 + \frac{I_{0,1}I_{1,2}I_{2,3}}{\mu_{0,1}\mu_{1,2}\mu_{2,3}}x_3)$. This reduces the system of ODEs for a tri-trophic food chain by one to a 3-dimensional system. That is, we restrict our attention to the dynamics on the invariant manifold. Then, the basin of attraction is a region in the positive cone $(x_1 \geq 0, x_2 \geq 0, x_3 \geq 0) \in \mathbb{R}^3_+$. Because $x_i \geq 0$ for $i = 0 \cdots 4$, the biologically feasible region is the interior of the tetrahedron, Ω, formed by the invariant planes $x_1 = 0$, $x_2 = 0$, $x_3 = 0$ such that

$$\Omega = \left\{(x_1, x_2, x_3)^T \in \mathbb{R}^3_+ : \frac{I_{0,1}}{\mu_{0,1}}x_1 + \frac{I_{0,1}I_{1,2}}{\mu_{0,1}\mu_{1,2}}x_2 + \frac{I_{0,1}I_{1,2}I_{2,3}}{\mu_{0,1}\mu_{1,2}\mu_{2,3}}x_3 \leq x_r\right\}. \tag{11}$$

The asymptotic behaviour of the system (2) can be understood by analysing the dynamics of orbits starting on the cross-section

$$\Sigma = \left\{(x_1, x_2, x_3)^T : x_1 > 0,\ x_2 = \frac{Dk_{2,3}}{\mu_{2,3} - D},\ x_3 > 0\right\} \tag{12}$$

Notice that $E_p \in \Sigma$ and the local extreme values of x_3 of the trajectories lie on Σ: Equation (2d) with $\frac{dx_3}{dt} = 0$ gives $x_2 = \frac{Dk_{2,3}}{\mu_{2,3}-D}$.

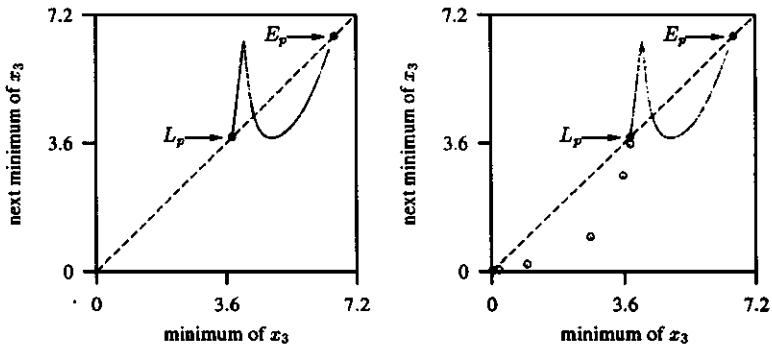

Figure 10: Next-minimum maps of system (2) without competition. In the left figure there is a chaotic attractor. In the right figure the chaotic attractor is destroyed by the collision between the chaotic attractor and the saddle limit cycle L_p (transient chaos). The last part of the trajectory to extinction is indicated by the symbol $\circ$.

The *Poincaré* or *next-return map* $P : \Sigma \to \Sigma$ is defined for a point $x \in \Sigma$ by $P(x) = \phi(\tau, x)$, where $\tau = \tau(x)$ is the time taken for the orbit $\phi(t, x)$ to first return to Σ. During one period the trajectory intersects Σ more than one time and an additional criterion (maximum or minimum of the top-predator) defines the map completely. This shows that for the model studied here the next-minimum map is in fact this next-return map. Similar as with the Marr-Pirt model, Figure 10, the next-return map calculated for the Monod model lies close to a single curve. One fixed point of this map is again the positive equilibrium E_p and the other represents the limit cycle L_p.

In the next subsections 5.1, 5.2 and 5.3 the three global bifurcations shown in Figure 7 are discussed.

5.1 Complex geometry of basin of attraction

The global heteroclinic bifurcation $G^{\neq}_{e,c}$ shown in Figure 7 is a tangency between the unstable manifold of a saddle-focus equilibrium E_p and the stable manifold of L_p along a non-transversal heteroclinic orbit [4, 5]. At this heteroclinic bifurcation, two heteroclinic orbits between E_p and L_p collide and disappear. These heteroclinic orbits are related to the basin of attraction of a positive attractor. An approximation of an heteroclinic orbit from x to y is obtained by solving the boundary-value problem such that $P^N(x)$ is close to y for N sufficiently large where $P(x)$ is the next-return map.

In Figure 11 the basin of attraction in the two-dimensional (x_1, x_3)-space is shown for two values of D. The concentration in the reservoir is now $x_r = 200$. The initial value of the predator density x_2 is set at its equilibrium value.

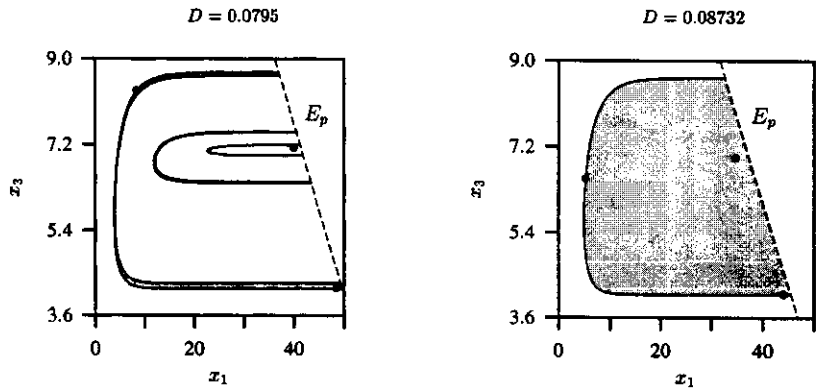

Figure 11: Basin of attraction for Monod model of tri-trophic food chain, system (2) with no competition and $m_i = 0$, $i = 1, 2, 3$ for $x_r = 200$. Orbits starting in the gray regions are asymptotic to a positive attractor. The solid curves are the boundaries of the basin of attraction. These solid curves are intersections of the two-dimensional stable manifold of L_p with Σ. The right-top bullet indicates the positive saddle-focus equilibrium E_p. The other two bullets are intersection points of the saddle cycle L_p with the hyperplane Σ defined in Equation (12).

In plane Σ the basin boundary is formed by the intersection of the stable manifold of L_p with Σ. The basin boundaries were calculated by a numerical continuation technique described in [5]. It was shown by numerical computation that the interior of the regions with the intersections of the stable manifold as boundary, form the basin of attraction. This was done by simulation, with initial points in the interior of the region.

Figure 12 is a one-parameter bifurcation diagram for the Monod model. The concentration in the reservoir is again $x_r = 200$. For different D values, the basin of attraction is obtained as the cross-sections of the basin of attraction such as shown in Figure 11 with the vertical line through the equilibrium point E_p. That is both the prey density x_1 and the predator density x_2 are set initially at their equilibrium values and the single scalar x_3 can be varied to study the basin of attraction. Notice that in Figure 12 the basin of attraction is shown for top-predator biomass density values below the equilibrium value. The resulting diagram is very much the same as in the one-dimensional diagram for the cubic map (10) given in Figure 3.

Moving through the bifurcation point $T_{c,3}$ by decreasing D, the saddle cycle L_p will disappear by the collision with a stable limit cycle. Hence, at this point $T_{c,3}$ also the heteroclinic orbits will disappear. Second, there is a global bifurcation point $G^{\neq}_{e,c}$, where two heteroclinic orbits collide and disappear.

If there are no heteroclinic orbits, an orbit starting in a small neighbourhood of E_p does not lead to disappearance of the top predator. In Figure 12 for D-values greater than the $G^{\neq}_{e,c}$ value,

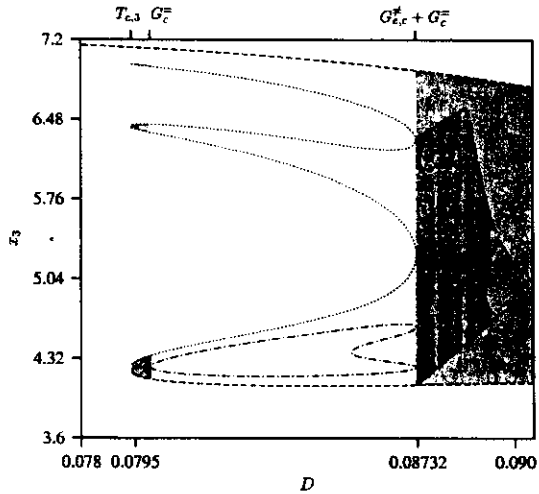

Figure 12: One-parameter bifurcation diagram for Monod model of tri-trophic food chain, system (2) with no competition and $m_i = 0$, $i = 1,2,3$, for $x_r = 200$. Plotted as points are the local minima of x_3 of the attractors versus D. The dashed curves indicate the equilibrium points and the minima for the limit cycle. Points on the dotted curves are heteroclinic points. Points on the dashed-dotted curve are homoclinic points. Starting at a point in the gray regions with the biomass density of the prey and predator in equilibrium and the biomass of the top-predator below its equilibrium value, is asymptotic to a strictly positive attractor. The homoclinic and heteroclinic bifurcation occur almost simultaneously indicated with $G_{e,c}^{\neq} + G_c^=$.

the basin of attraction is a connected region around the equilibrium values of the top-predator x_3 (see also Figure 11 with $D = 0.08732$).

In contrast, if there are heteroclinic orbits for D-values between the bifurcations $T_{c,3}$ and $G_{e,c}^{\neq}$, starting near E_p can possibly lead to extinction of the top-predator. In Figure 12 for D-values between the bifurcations $G_c^=$ and $G_{e,c}^{\neq} + G_c^=$ there is almost always extinction of the top-predator except for the homoclinic and heteroclinic orbits. With D-values between the bifurcations $G_c^=$ and $T_{c,3}$ there are also positive attractors, limit cycles or chaotic attractors. The basin of attraction has a complex geometry close to the equilibrium value. There are disconnected intervals for x_3 which converge to the positive attractor alternated with intervals where the top-predator goes extinct (see also Figure 11 with $D = 0.0795$). The lengths of both types of intervals converge to zero when approaching the equilibrium value for x_3. At the tangent bifurcation $T_{c,3}$ the basin boundary is formed by vertical lines with constant D. With raising the D-value the distance between the chaotic attractor and its basin boundary decreases until at the global homoclinic

bifurcation $G_c^=$ value they touch. This is called a boundary crisis and this is subject of the next section 5.2.

These results show that with the calculation of a one-dimensional bifurcation diagram the initial condition for each value of the bifurcation parameter has to be chosen carefully. With the calculation of the one-dimensional bifurcation diagram the bifurcation parameter is varied step-wise. Then small perturbations from the equilibrium value used as an initial point can yield irregular results when heteroclinic orbits exists: sometimes there is convergence to a positive attractor and sometimes extinction of the top-predator. In Figures 9 and 12, for each value of the bifurcation parameter integration in time was started from the attractor for slightly different values of the bifurcation parameter. Starting conditions for the first bifurcation parameter value are obtained from continuation in the two-dimensional bifurcation parameter plane where a bifurcation curve is continued from a point in the bifurcation diagram where the dynamics is simple.

5.2 Boundary crisis

Figures 9 and Figure 12 show that a chaotic attractor and its basin of attraction are destroyed by the collision between the chaotic attractor and the coexisting saddle cycle L_p; see also [17, 50]. Grebogi, Ott and Yorke [17, 18] called this a *boundary crisis*. McCann and Yodzis [41,42] found similar crises for a tri-trophic food chain where the lowest trophic level grows logistically. The "hole" in the chaotic attractor between the global bifurcations $G_c^=$ in Figure 9 resembles that depicted in [41, Figure 2], calculated for a tri-trophic food chain with viable lowest trophic level. At the crisis, the chaotic behaviour converts into a chaotic transient. That is, with simulation in time the flow follows, possibly for a long time, the ghost of a chaotic attractor but finally the top-predator disappears (see Figure 10).

This boundary crisis is associated with the homoclinic bifurcation. An approximation of an homoclinic orbit to x is obtained by solving the boundary-value problem such that $P^N(x)$ is close to x for N sufficiently large where $P(x)$ is again the next-return map. The intersection of a homoclinic orbit with Σ is called a homoclinic point. If $x \in \Sigma$ is a homoclinic point then $P^n(x)$ is a homoclinic point for each $n \geq 1$. Similar to the homoclinic orbits for the cubic map (10) given in Figure 3, for D-values between the bifurcations $G_c^=$ and $G_{e,c}^{\neq} + G_c^=$ in the one-parameter diagram Figure 12, only the homoclinic points x for which $P^2(x)$ is sufficiently close to the fixed point of the next-return map, are depicted. At the homoclinic bifurcation point $G_c^=$, the stable and unstable manifold of a saddle cycle L_p are tangent along a non-transversal homoclinic orbit. Figure 12 shows that at this homoclinic bifurcation point there are two pairs of homoclinic orbits which collide and disappear. The study of the cubic map (10) with α-values slightly less than 0.8 (see also Figure 2), gives insight in this phenomenon; for a complete discussion the reader is referred to [5].

5.3 Episodes close to an unstable equilibrium

There are homoclinic orbits to the saddle-focus equilibrium E_p. These orbits spend large amounts of time close to the unstable equilibrium separated by large excursions of the orbit through the

state space. The Marr-Pirt system (2), without the competitor $x_{12} = 0$, is four-dimensional and the Jacobian matrix evaluated in the unstable equilibrium has one pair of complex conjugated eigenvalues with positive real parts while the other two eigenvalues are negative in the region of the (x_r, D)-plane bounded by the Hopf bifurcation curve H_3^-. Moreover, the real eigenvalues have larger magnitude than the real parts of the complex conjugated eigenvalues. The homoclinic orbits spiral outward along the two-dimensional unstable manifold and approach the equilibrium along the one-dimensional stable manifold corresponding to the leading negative eigenvalue closest to the imaginary axis.

This global Shil'nikov bifurcation forms a 'skeleton' for the period doubling of which a cascade leads to chaotic dynamics. There is no catastrophic destruction of the chaotic attractor and its basin of attraction with this type of global bifurcation. This bifurcation is accessible by following a single periodic orbit and a countable infinity of periodic orbits appears in a cascade of periodic-doubling and tangent bifurcations, [19,29].

In Figure 10 the next-minimum map of x_3 has a maximum value close to the equilibrium value for E_p. This indicates that the bifurcation parameter values are close to the homoclinic bifurcation curve $G_e^=$ shown in Figure 9 where the chaotic attractor touches the unstable equilibrium. From this diagram we conclude that at the homoclinic bifurcation to the saddle-focus equilibrium E_p the local maximum and minimum lines of the biomass of the top-predator touch the equilibrium curve E_p. In Figure 12 the chaotic attractor does not touch the unstable equilibrium; indeed there is no Shil'nikov bifurcation for the Monod model in the region of the bifurcation diagram studied, as is explained in [29].

This shows that the next-minimum map, and this is also true for the next-maximum map, can be used to detect a homoclinic bifurcation curve for the saddle-focus equilibrium, but that the analogy between the dynamics of the map and the flow fails to hold.

6 Simple food web

We discuss the dynamics of system (2) in the positive cone $(x_0 \geq 0, x_{11} \geq 0, x_{12} \geq 0, x_2 \geq 0) \in \mathbf{R}^4_+$, thus without a top-predator. In [52] also a web with the trophic graph given in Figure 1.b under chemostat conditions was analyzed using bifurcation analysis. The Monod model was used, that is, no maintenance $m_{ij} = 0, i, j = 1, 2$. Chaotic behaviour resulting from successive period doublings was observed. Multi-stability phenomena of coexistence of equilibria and limit cycles at the same operating conditions were also found. Here we will analyse the influence of a predator on the dynamics of the two competing prey population connected to competitive exclusion.

6.1 Competitive exclusion

We will consider a specific competitor prey, x_{12}. The maximum growth rate of the competitor, $\mu_{0,12}$, is smaller than that of the prey, $\mu_{0,11}$, while the maximum growth rate of the predator consuming the competitor, $\mu_{12,2}$, is larger than the maximum growth rate of the predator consuming the prey, $\mu_{11,2}$; see Table III.

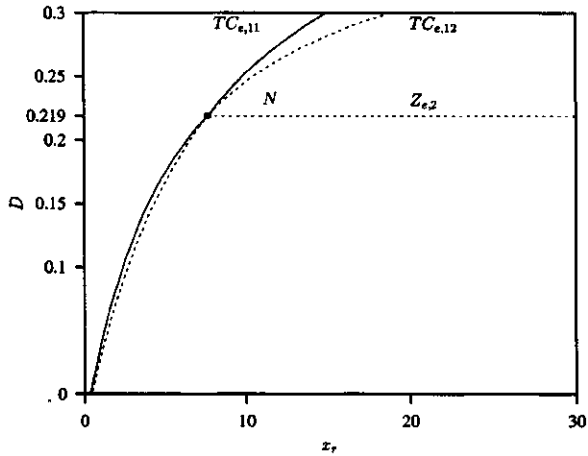

Figure 13: Bifurcation diagram for Marr-Pirt model of nutrient–prey–competitor system (2) without predation $x_2 = x_3 = 0$. The bifurcation parameters are the dilution rate D and the substrate concentration in reservoir x_r. Values assigned to physiological parameters and reference values for the perturbation parameters are listed in Table III. The curves $TC_{e,11}$, $TC_{e,12}$ mark transcritical bifurcations. Point N is a codimension 2 point. The bifurcation curve $Z_{e,2}$ originates from this point. The solid parts of the transcritical bifurcation curves are relevant when both prey and competitor are possible invaders.

Nutrient–prey–competitor There is competition between the prey species for a common nutrient. This system, thus in the absence of the predator, $x_2 = 0$, is already dealt with extensively in [49]. Here we will confine ourselves to explaining the bifurcation diagram.

The bifurcation diagram of the nutrient–prey–competitor system is shown in Figure 13. There is a bifurcation curve denoted by $Z_{e,2}$ where one eigenvalue equals zero. It originates from the codimension 2 point N, the intersection point of the two (supercritical) transcritical bifurcation curves $TC_{e,11}$ and $TC_{e,12}$.

The critical dilution rate, denoted by D^*, is determined by the condition that the growth rate for the two competitors consuming the common nutrient, is the same. For $D = D^*$ there is coexistence. When the dilution rate is above the critical value, $D > D^*$, the prey always wins and the relevant transcritical bifurcation curve is $TC_{e,11}$, while for $D < D^*$ the competitor always wins, that is, it establishes itself and eliminates the prey and the relevant transcritical bifurcation curve is $TC_{e,12}$.

Nutrient–two-prey–predator Now we discuss the bifurcation diagram for the bi-trophic food web including the predator $x_2 > 0$. Here we emphasize only the dynamic behaviour close to the

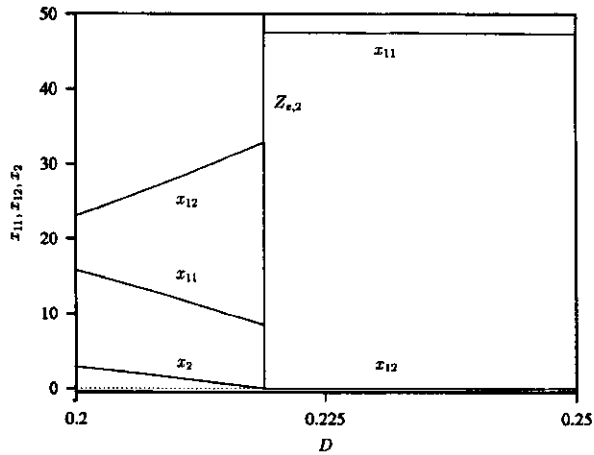

Figure 14: One-parameter bifurcation diagram for Marr-Pirt model with equilibrium values of the prey populations x_{11} and x_{12} and predator x_2. The bifurcation parameter is the dilution rate D. The concentration in the reservoir is $x_r = 140$.

bifurcation curve $Z_{e,2}$ where $D = D^*$; for a complete discussion the reader is referred to [32].

Figure 14 gives the one-parameter bifurcation diagram where x_r is fixed and the consequences for the abundance of the species when the dilution rate is varied, are displayed. The biomass densities for the two competing prey species x_{11} and x_{12} are discontinuous at $D = D^*$. Observe that for $D = D^*$ the equilibrium values for these two state variables are not unique and all points on an one-dimensional manifold are equilibrium points. For $D < D^*$ there is coexistence of the three species and for $D > D^*$ the prey always wins, that is $x_{12} = 0$ as well as $x_2 = 0$.

7 Discussion and conclusions

We showed that cyclic dynamics of autonomous continuous-time systems can have essential features of the dynamics of a one-dimensional discrete-time system. The relation between the food chain model and the one-dimensional map can be made clear by constructing a next-return map. As in the Lorenz system [36], with chaotic behaviour all points appear to lie close to single curve; see Figure 10. Thus the peak value of x_3 on one turn appears to be almost uniquely determined by the peak value on the previous turn, [50]. This relationship is used to clarify global bifurcations of the food chain model, including boundary crises and complex geometry of

the basin of attraction of a strange attractor.

The information of one- and two-parameter bifurcation diagrams is presented in one figure; see for example Figure 8. This minimizes the overlook of relevant bifurcations.

We distinguish three types of asymptotic behaviour of tri-trophic food chains (Figure 1.a): stable coexistence, bi-stability, and extinction of the top-predator for almost all positive initial conditions. Increasing the concentration of input substrate x_r for a bi-trophic food chain (see Figure 5) can cause destabilisation of the otherwise stable equilibrium (paradox of enrichment). For a tri-trophic food chain the increase of the nutrient supply at the bottom of the food chain can even lead to disappearance of the highest trophic level (see Figure 6 and 8), since an abundance of nutrients for the lowest trophic level leads to strong oscillations between prey and predator, which is unfavourable for the top-predator population.

The Shil'nikov global bifurcation curve forms a 'skeleton' for the period doubling of which a cascade leads to chaotic dynamics. The homoclinic bifurcation to a saddle limit cycle is associated with a boundary crisis where the strange attractor is abruptly destroyed. Heteroclinic orbits from a saddle-focus equilibrium to a saddle limit cycles, form the basin boundary for positive attractors, that is periodic orbits and strange attractors. Close to the equilibrium there is a complicated geometry of the basin of attraction. This phenomenon has to be taken into account with the construction of one-dimensional bifurcation diagrams. Starting from a perturbed equilibrium can yield misleading results. Therefore, in a continuation process we started from the attractor for slightly different values of the bifurcation parameter. In [28] this technique was also applied when multiple attractors coexist.

There is a point denoted by G in Figure 7 for the intersection of the homoclinic bifurcation curves $G_e^=$ with the heteroclinic bifurcation curve $G_{e,c}^{\neq}$. With the Marr-Pirt model the dimension of the state space is four. At the saddle-focus equilibrium E_p there are two negative real eigenvalues and two complex conjugated eigenvalues of the Jacobian with positive real part. The homoclinic orbit at the Shil'nikov bifurcation $G_e^=$ spirals outward along the two-dimensional unstable manifold and approaches the equilibrium E_p along the one-dimensional stable manifold corresponding to the leading negative eigenvalue closest to the imaginary axis [29]. The degenerated heteroclinic orbit in $G_{e,c}^{\neq}$ spirals also outward along the two-dimensional unstable manifold of E_p but approaches the coexisting limit cycle L_p along an one-dimensional stable manifold.

In the neighbourhood of the point G the geometry of the basin of attraction, discussed in relationship with the heteroclinic orbits from the saddle-focus equilibrium to the limit cycle, will be even more complex. This is because there are an infinite number of tangent and flip bifurcations associated with the homoclinic Shil'nikov global bifurcation to the saddle-focus equilibrium and therefore also an infinite number of intervals where stable long-periodic orbits exist.

Here we studied the basin of attraction only for the Monod model and in [29] we showed that there is no Shil'nikov bifurcation for the Monod model in the part of the bifurcation parameter space studied here. Therefore in this paper we do not see this interaction. A discussion of the basin of attraction for positive attractors with the Marr-Pirt model is beyond the scope of this paper, but the results will be similar to those obtained here for the Monod model.

The importance of the global homoclinic bifurcations is the connection with chaotic behaviour. Klebanoff and Hastings [27] studied the normal form of a bifurcation point M_1 in

the tri-trophic food chain where the lowest level grows logistically. They associated the origin of chaos with this bifurcation point. Kuznetsov and Rinaldi [34] showed that chaos arises in a region far from M_1 of the parameter space. In [42] homoclinic orbits of the Shil'nikov type were shown to be related to a strange attractor. This agrees with our results for the Marr-Pirt tri-trophic food chain model. For the Monod model this is only the case when a Shil'nikov bifurcation occurs outside the part of the bifurcation space with $0 \leq x_r \leq 300$ studied in [29] where no Shil'nikov bifurcation for the Monod model was found.

With two competing species competitive exclusion holds, that is, generally one prey population wins. Bifurcation analysis is used to shown the consequence of the introduction of a predator (Figure 1.b). The degenerated case where without a predator both competing species coexist, marks a bifurcation point where the equilibrium biomass densities of the species can be discontinuous when the bifurcation parameter in varied.

The bifurcation analysis of the full system (2) is beyond the scope of this paper, but in order to analyse its dynamics, study of the following subwebs is essential:

- One food chain with only one trophic level, the classical chemostat situation: ($x_{21} = 0, x_{22} = 0, x_3 = 0$).
- Two bi-trophic food chains: ($x_{21} = 0, x_3 = 0$), ($x_{22} = 0, x_3 = 0$).
- One bi-trophic food web: ($x_3 = 0$).
- Two tri-trophic food chains: ($x_{21} = 0$), ($x_{22} = 0$).

The bifurcation analysis of these food web structures is discussed in this paper.

All the models studied in this paper have been concerned with ecosystems with a few interacting species, and the question naturally arises as to what happens when more realistic details and additional species are introduced into the models (see [23]). At present it remains an open question whether multi-species ecosystems are more stable than ecosystems with only a few species, as is often suggested in the literature. In principle, bifurcation theory can be used to answer this question. However, for large-scale food webs containing many state variables and many parameters it is impractical to calculate the full bifurcation diagram with respect to all types of nutrient import and export rates. For, the calculation of the bifurcation points may be troublesome due to the large dimension of the underlying (often stiff) non-linear dynamic system.

Acknowledgements

The authors would like to thank Wim van der Steen for corrections in the manuscript.

References

[1] W.-J. Beyn, The numerical computation of connecting orbits in dynamical systems, *IMA J. Num. Anal.* 9 (1990) 379–405.

[2] W.-J. Beyn and J.-M. Kleinkauf, The numerical computation of homoclinic orbits for maps, *SIAM J. Numer. Anal.* 34 (1997) 1207–1236.

[3] M. P. Boer, *The dynamics of tritrophic food chains*, Ph.D. thesis, Vrije Universiteit, de Boelelaan 1087, 1081 HV Amsterdam, The Netherlands (2000).

[4] M. P. Boer, B. W. Kooi, and S. A. L. M. Kooijman, Food chain dynamics in the chemostat, *Mathematical Biosciences* 150 (1998) 43–62.

[5] M. P. Boer, B. W. Kooi, and S. A. L. M. Kooijman, Homoclinic and heteroclinic orbits in a tri-trophic food chain, *Journal of Mathematical Biology* 39 (1999) 19–38.

[6] A. R. Champneys and Y. A. Kuznetsov, Numerical detection and continuation of codimension-two homoclinic bifurcations, *Int. Journal of Bifurcation and Chaos* 4 (1994) 795–822.

[7] A. R. Champneys, Y. A. Kuznetsov, and B. Sandstede, A numerical toolbox for homoclinic bifurcation analysis, *Int. Journal of Bifurcation and Chaos* 6 (1996) 867–887.

[8] A. R. Champneys and G. J. Lord, Computation of homoclinic solutions to period orbits in a reduced water-wave problem, *Physica D* 102 (1997) 101–124.

[9] A. Cunningham and R. M. Nisbet, Transients and oscillations in continuous culture, in M. J. Bazin, ed., *Mathematics in Microbiology*, Academic Press, London (1983) pp. 77–103.

[10] O. De Feo and S. Rinaldi, Singular homoclinic bifurcations in tri-trophic food chains, *Mathematical Biosciences* 148 (1998) 7–20.

[11] W. de Melo and S. van Strien, *One-Dimensional Dynamics*, Springer-Verlag (1993).

[12] A. M. De Roos, J. A. J. Metz, E. Evers, and A. Leipoldt, A size dependent predator-prey interaction: who pursues whom?, *Journal of Mathematical Biology* 28 (1990) 609–643.

[13] R. L. Devaney, *An Introduction to Chaotic Dynamical Systems*, Addison-Wesley, Redwood City, CA (1989).

[14] O. Diekmann, S. D. Mylius, and J. R. ten Donkelaar, Saumon à la Kaitala et Getz, sauce hollandaise, *Evolutionary Ecology Research* 1 (1998) 261–275.

[15] E. J. Doedel, A. R. Champneys, T. F. Fairgrieve, Y. A. Kuznetsov, B. Sandstede, and X. Wang, *AUTO 97: Continuation and Bifurcation software for ordinary differential equations*, Technical report, Concordia University, Montreal, Canada (1997).

[16] M. E. Gilpin, Spiral chaos in a predator prey model, *The American Naturalist* 107 (1979) 306–308.

[17] C. Grebogi, E. Ott, and J. A. Yorke, Crises, sudden changes in chaotic attractors, and transient chaos, *Physica D* 7 (1983) 181–200.

[18] C. Grebogi, E. Ott, and J. A. Yorke, Fractal basin boundaries, long-lived chaotic transients and unstable–unstable pair bifurcation, *Phys. Rev. Lett.* 50 (1983) 935–938.

[19] J. Guckenheimer and P. Holmes, *Nonlinear Oscillations, Dynamical Systems and Bifurcations of Vector Fields*, volume 42 of *Applied Mathematical Sciences*, Springer-Verlag, New York, 2 edition (1985).

[20] A. Hastings, What equilibrium behaviour of Lotka-Volterra models does not tell us about food webs, in G. A. Polis and K. O. Winemiller, eds., *Food webs*, Chapman & Hall, New York (1996) pp. 211–217.

[21] A. Hastings and T. Powell, Chaos in a three-species food chain, *Ecology* 72 (1991) 896–903.

[22] J. Hofbauer and K. Sigmund, *The Theory of Evolution and Dynamical Systems*, Cambridge University Press, Cambridge (1988).

[23] F. C. Hoppensteadt, *Topics in Nonlinear Dynamics, Applications to Physics, Biology and Economic Systems*, World Scientific, Singapore (1996).

[24] V. Kaitala, J. Ylikarjula, and M. Heino, Dynamic complexities in host-parasitoid interaction, *Journal of Theoretical Biology* 197 (1999) 331–341.

[25] A. I. Khibnik, Y. A. Kuznetsov, V. V. Levitin, and E. V. Nikolaev, Continuation techniques and interactive software for bifurcation analysis of ODEs and iterated maps, *Physica D* 62 (1993) 360–371.

[26] A. Klebanoff and A. Hastings, Chaos in one-predator, two-prey models: General results from bifurcation theory, *Mathematical Biosciences* 122 (1994) 221–233.

[27] A. Klebanoff and A. Hastings, Chaos in three-species food chain, *Journal of Mathematical Biology* 32 (1994) 427–451.

[28] B. W. Kooi, M. P. Boer, and S. A. L. M. Kooijman, Complex dynamic behaviour of autonomous microbial food chains, *Journal of Mathematical Biology* 36 (1997) 24–40.

[29] B. W. Kooi, M. P. Boer, and S. A. L. M. Kooijman, Consequences of population models on the dynamics of food chains, *Mathematical Biosciences* 153 (1998) 99–124.

[30] B. W. Kooi, M. P. Boer, and S. A. L. M. Kooijman, On the use of the logistic equation in food chains, *Bulletin of Mathematical Biology* 60 (1998) 231–246.

[31] B. W. Kooi, M. P. Boer, and S. A. L. M. Kooijman, Resistance of a food chain to invasion by a top predator, *Mathematical Biosciences* 157 (1999) 217–236.

[32] B. W. Kooi and S. A. L. M. Kooijman, Invading species can stabilize simple trophic systems, *Ecological Modelling* 133 (2000) 57–72.

[33] Y. A. Kuznetsov, *Elements of Applied Bifurcation Theory*, volume 112 of *Applied Mathematical Sciences*, Springer-Verlag, New York (1995).

[34] Y. A. Kuznetsov and S. Rinaldi, Remarks on food chain dynamics, *Mathematical Biosciences* 124 (1996) 1–33.

[35] R. Law and R. D. Morton, Permanence and the assembly of ecological communities, *Ecology* 77 (1996) 762–775.

[36] E. N. Lorenz, Deterministic non-periodic flow, *Journal of Atmospheric Science* 20 (1963) 130–141.

[37] R. S. MacKay and C. Tresser, Some flesh on the skeleton: the bifurcations of bimodal maps, *Physica D* 27 (1987) 412–422.

[38] R. M. May, Biological populations with non-overlapping generations: stable points, stable cycles and chaos, *Science* 186 (1974) 645–647.

[39] R. M. May, Simple mathematical models with vary complicated dynamics, *Nature* 261 (1976) 459–467.

[40] R. M. May and G. Oster, Bifurcations and dynamic complexity in simple ecological models, *The American Naturalist* 110 (1976) 573–599.

[41] K. McCann and P. Yodzis, Nonlinear dynamics and population disappearances, *The American Naturalist* 144 (1994) 873–879.

[42] K. McCann and P. Yodzis, Bifurcation structure of a tree-species food chain model, *Theoretical Population Biology* 48 (1995) 93–125.

[43] J. A. J. Metz and O. Diekmann, *The dynamics of physiologically structured populations*, volume 68 of *Lecture Notes in Biomathematics*, Springer-Verlag, Berlin (1986).

[44] R. D. Morton and R. Law, Regional species pools and the assembly of local ecological communities, *Journal of Theoretical Biology* 187 (1997) 321–331.

[45] H. T. Odum, *Ecological and General Systems: An Introduction to System Ecology*, University press of Colorado (1984).

[46] W. E. Ricker, Stock and recruitment, *J. Fish. Res. Bd. Can.* 11 (1954) 559–623.

[47] M. L. Rosenzweig and R. H. MacArthur, Graphical representation and stability conditions of predator-prey interactions, *The American Naturalist* 97 (1963) 209–223.

[48] D. Singer, Stable orbits and bifurcation of maps of the interval, *SIAM J. Appl. Math.* 35 (1978) 260–267.

[49] H. L. Smith and P. Waltman, *The Theory of the Chemostat*, Cambridge University Press, Cambridge (1994).

[50] J. M. T. Thompson and H. B. Stewart, *Nonlinear Dynamics and Chaos*, John-Wiley (1986).

[51] S. J. van Strien, *Structures in Dynamics*, Elsevier (1991) pp. 111–160.

[52] D. V. Vayenas and S. Pavlou, Chaotic dynamics of a food web in a chemostat, *Mathematical Biosciences* 162 (1999) 69–84.